Dynamics of n-alkanes: Comparison to Rouse Model

Maurizio Mondello, Gary S. Grest, Edmund B. Webb III, P. Peczak, and Scott T. Milner

Corporate Research Science Laboratories, Exxon Research and Engineering Company, Annandale, New Jersey 08801

(February 2, 2008)

Abstract

The crossover to Rouse-like behavior for the self-diffusion constant D, the viscosity η, and the equilibrium structural statistics of n-alkanes ($6 \leq n \leq 66$) is studied numerically. For small n the chains are non-Gaussian and the mean squared end-to-end distance $\langle R^2 \rangle$ is greater than $6\langle R_G^2 \rangle$, where $\langle R_G^2 \rangle$ is the mean squared radius of gyration. As n increases, $\langle R^2 \rangle / \langle R_G^2 \rangle \to 6(1 + a/n)$, where a depends on the interaction model. At constant density, the Rouse model is used to extract the monomeric friction coefficient ζ and the viscosity η independently from the diffusion constant D and the longest relaxation time τ_R. ζ_D extracted from D is nearly independent of chain length while ζ_τ obtained from τ_R is much larger than ζ_D for small n. The viscosity measured in a non-equilibrium molecular dynamics simulation is closely approximated by the value of η determined from τ_R while η inferred from D is smaller for small n. For $n \gtrsim 60$, the two estimates for both ζ and η agree as predicted from the Rouse model. D calculated from three interaction models is studied for increasing n and compared to experimental data.

I. INTRODUCTION

It is well known that dynamics of a melt of unentangled polymer chains satisfies the Rouse model [1] exceedingly well. For chains which are shorter than an entanglement length n_e, the self-diffusion constant and viscosity for a melt of chains of length n are observed experimentally [2,3] to scale as n^{-1} and n, respectively, as predicted by the Rouse model. Computer simulations on simple bead spring models [4] have shown that not only does the Rouse model predict the correct scaling dependence on chain length n, it also gives quantitatively correct results. Why this simple model, which was first proposed [1] to model the dynamics of dilute polymer solutions, works so well for a polymer melt remains somewhat of a mystery.

The crossover from Rouse-like behavior for unentangled short chains to reptation-like motion for entangled chains has received considerable attention in recent years, while the crossover from the behavior of very small molecules to the Rouse regime has received relatively little attention. Understanding the latter crossover can provide information on subtleties of the Rouse model and at the same time increase knowledge on the dynamics of a technologically important class of molecules, normal alkanes. There have been a number of studies of the dynamics of short alkanes, but to our knowledge there have been no systematic studies which examine the dependence of either the diffusion or viscosity on chain length. One can also examine the crossover of the mean squared radius of gyration $\langle R_G^2 \rangle$ and end-to-end distance $\langle R^2 \rangle$ as a function of n. For Gaussian chains, $\langle R_G^2 \rangle$ and $\langle R^2 \rangle$ satisfy

$$\langle R^2 \rangle = 6\langle R_G^2 \rangle = nb^2 \tag{1}$$

where b is the effective bond length. Consider the simple case of normal alkanes, though the same is true for any flexible chain molecule: for small n, the chains are clearly non-Gaussian and $\langle R^2 \rangle > 6\langle R_G^2 \rangle$. For normal n-alkanes, crossover to Gaussian chain statistics occurs for n greater than 100 [5,6,7]. Since the Rouse model is based on the fact that the chains are Gaussian, one would expect that crossover length is a minimum chain length for the Rouse model to hold, though this has not previously been checked systematically.

In the Rouse model, the excluded volume interactions and the hydrodynamic interactions are disregarded and the polymer is treated as a collection of beads connected with a harmonic spring with spring constant $k = 3k_BT/b^2$. Here T is the temperature and k_B is Boltzmann's constant. The dynamics of the chain is then modeled with a Langevin equation with a monomeric friction coefficient ζ. The resulting set of equations can be solved by transforming to normal coordinates. The resulting self-diffusion constant is [8]

$$D = \frac{k_BT}{n\zeta}. \tag{2}$$

The rotational relaxation time τ_R of a polymer is usually defined by the longest relaxation time of the end-to-end autocorrelation function $\langle \mathbf{R}(t) \cdot \mathbf{R}(0) \rangle$ and expressed as [8],

$$\tau_R = \frac{\zeta n^2 b^2}{3\pi^2 k_B T}. \tag{3}$$

The effective bond length b can be eliminated in favor of either $\langle R^2 \rangle$ or $\langle R_G^2 \rangle$ using eq. 1,

$$\tau_R = \frac{\zeta n \langle R^2 \rangle}{3\pi^2 k_B T} = \frac{2\zeta n \langle R_G^2 \rangle}{\pi^2 k_B T}. \tag{4}$$

The viscosity η of a melt can be determined from the relaxation modulus $G(t)$, which can be written as a sum over the Rouse modes of a chain. In terms of τ_R [8],

$$\eta = \frac{\pi^2 \rho R T \tau_R}{12M}, \tag{5}$$

where M is the molecular weight, ρ is the density, and R is the gas constant. This gives the well known result that for Rouse chains, the viscosity scales linearly with n for constant monomeric friction coefficient. This simple scaling does not hold at constant temperature and pressure, since ρ and therefore ζ increase with increasing n. This results in a stronger dependence on n, namely $\eta \sim D^{-1} \sim n^{-1.8}$ for unentangled polyethylene chains for $T = 448$ K [9].

To study the crossover from small molecule behavior to Rouse-like chains, it is convenient to rewrite the monomeric friction coefficient ζ and viscosity η in several different forms. From eq. 2 for the diffusion constant D, we can write

$$\zeta_D = \frac{k_B T}{nD}. \tag{6}$$

From eq. 4 for the rotational relaxation time τ_R, we have two measures of ζ depending on whether we use $\langle R^2 \rangle$ or $\langle R_G^2 \rangle$ to eliminate b,

$$\begin{aligned} \zeta_\tau(R) &= \frac{3\pi^2 k_B T \tau_R}{n\langle R^2 \rangle} \\ \zeta_\tau(R_G) &= \frac{\pi^2 k_B T \tau_R}{2n\langle R_G^2 \rangle}. \end{aligned} \tag{7}$$

The viscosity can also be written three different ways. The first, given by eq. 5, we refer to as η_τ. Two additional expressions for η in terms of D, can be obtained by substituting each form of eq. 4 for τ_R in eq. 5 and eliminating ζ in favor of D using eq. 2,

$$\begin{aligned} \eta_D(R) &= \frac{\rho RT \langle R^2 \rangle}{36MD} \\ \eta_D(R_G) &= \frac{\rho RT \langle R_G^2 \rangle}{6MD}. \end{aligned} \tag{8}$$

These three expressions for both ζ and η are equivalent for Rouse chains, so that any differences are a clear signature of deviations from Rouse behavior.

To investigate the crossover to Rouse-like chains with increasing chain length, we carried out a series of equilibrium (EMD) and non-equilibrium molecular dynamics (NEMD) simulations for normal alkanes with $6 \leq n \leq 66$ at the density for high molecular weight polyethylene. Constant density was studied due to the large corrections to Rouse behavior observed experimentally for unentangled chains below the entanglement length n_e at atmospheric pressure. The EMD simulations were used to calculate both ζ and η as predicted by the three expressions for each discussed above. The results for η, as predicted by the EMD calculations, were compared to the viscosity calculated directly from the NEMD simulations. We also carried out EMD simulations on alkanes in this size range employing three different interaction models discussed recently in the literature. These were performed at experimental density for atmospheric pressure and the diffusion constant D as a function

of chain length was compared to experiment. All sets of EMD simulations were used to study the behavior of the equilibrium structural statistics $\langle R_G^2 \rangle$ and $\langle R^2 \rangle$ with increasing chain length. To efficiently extend this comparison out to sizes larger than $n = 66$, we also carried out simulations using the rotational isomeric state (RIS) model for chains in the range $34 \leq n \leq 2000$.

In Sec. II we summarize the simulation models and the methodology used. The equilibrium results for the static structural properties and their behavior with increasing n are presented in Sec. III. Results for the dynamics are presented in Sec. IV where we discuss the crossover for the monomeric friction coefficient and viscosity as a function of chain length n and compare diffusion results to experiment and predictions based on the Rouse model. We briefly summarize our main conclusions in Sec. V.

II. SIMULATION MODEL AND METHOLOGY

In order to study a wide range of chain lengths, an united atom (UA) model was used to simulate the linear alkanes. In this model, the hydrogen atoms are not explicitly simulated. Rather, they are grouped with the carbon to which they are bonded into a single particle or a united atom. We do, however, distinguish between different CH_n groups. These groups or united atoms interact through bonded and non-bonded forces. The bonded interactions are represented by constraint forces which keep intramolecular nearest-neighbors at a fixed distance, a bending term

$$V_b(\theta) = \frac{k_b}{2}(\theta - \theta_b)^2 \tag{9}$$

where θ_b is the equilibrium angle between successive bonds, and a torsional term

$$V_t(\phi) = \sum_i a_i \cos^i(\phi) \tag{10}$$

characterizing preferred orientations and rotational barriers around all non-terminal bonds. The non-bonded forces are described by Lennard-Jones (LJ) interaction sites located at the position of each carbon atom center of mass. The LJ potential is defined by

$$V_{LJ}(r) = 4\epsilon[(\frac{\sigma}{r})^{12} - (\frac{\sigma}{r})^6] \tag{11}$$

This non-bonded interaction is between both intermolecular and intramolecular sites except for those which are separated by less than four bonds and which therefore interact through one or more of the bonded interaction terms. The LJ interaction is usually truncated at a distance r_c and the potential shifted so that $V_{LJ}(r_c) = 0$.

In our earlier studies of the diffusion [10,11] and viscosity [12] of linear and branched alkanes, we studied two models for the interactions. The first was the symmetric UA model of Siepmann *et al.* [13,14] which was developed to describe the vapor-liquid coexistence curves of the n-alkane phase diagram [15]. We refer to this as model A. The second, which we denote as model B, was the asymmetric united atom (AUA) model of Padilla and Toxvaerd [16,17] which was optimized to describe the static and dynamic behavior of short n-alkanes ($5 \leq n \leq 10$) at moderately high temperatures and pressures. In this latter model, there is a displacement between the centers of force of non-bonded interactions and the centers of mass of the united atoms, hence the name. Paul *et al.* [18] recently introduced a new, optimized symmetric UA model which they claimed was better able to reproduce the properties of melts of linear normal alkanes. The primary differences between their model and that of Siepmann *et al.* [13,14] was the use of a slightly larger σ and a different torsional potential; we refer to our implementation of this last parameterization as model C [19].

The intramolecular interaction parameters for the three models are listed in Table I. The parameters for the torsional potential of model A are from Jorgensen *et al.* [20]. Paul *et al.* [18] presented results for two torsional potentials. The first one they studied gave a diffusion constant which was 45% larger than the experimental result for $n - C_{44}H_{90}$ at $T = 400$ K. They subsequently modified the torsional potential $V_t(\phi)$ to increase the *trans-gauche* barrier from 3.0 to 3.3 kcal/mol. Since this latter model gave a better estimate of the D, though still 30% too large for $n - C_{44}H_{90}$, we used their modified version of $V_t(\phi)$ here. For comparison, the torsional potentials for the three models are shown in Fig. 1. Note that the *gauche* energy is about the same for models B and C (0.5 kcal/mol) and about half that of model A (0.9 kcal/mol). This difference will influence the thermodynamic flexibility of the molecules and the persistence length for long chains. Models B and C are expected to

result in more thermodynamically flexible molecules than model A. The dynamic flexibility is related to the size of the *trans-gauche* barrier, which is larger for model B than for models A and C. Thus, models A and C lead to more dynamically flexible molecules than model B.

The Lennard-Jones parameters are listed in Table II for all three models. Note that the interaction strength ϵ is the same for models A and C. The effective diameter for the united atoms is different for the three models, with model C having a larger effective diameter than model A. For model B, a direct comparison based on the value of σ is not appropriate due to the asymmetric nature of united atoms. While the σ for model B is the smallest, the displacement between the center of force of non-bonded interactions and the center of mass of the united atom, results in an effectively larger united atom than represented by σ. The interaction parameter between a CH_3 and CH_2 site is given by the Lorenz-Bertholot rule, $\sqrt{\epsilon_{CH_3}\epsilon_{CH_2}}$. We used a 10 $\mathring{A}$ cutoff for the (shifted) LJ potential.

All of the MD results presented here were obtained from constant volume, constant temperature simulations. The velocity rescaling algorithm of Berendsen *et al.* [21] was used to control the temperature in the EMD simulations while the Nose-Hoover [22] algorithm was used for the NEMD simulations. The equations of motion were integrated using the velocity Verlet algorithm [22] with a 5 fs time step for both the EMD and NEMD simulations. Bond lengths were kept constant using the RATTLE algorithm [22,23]. Equilibrium structural statistics, the self-diffusion constant D, and rotational diffusion time τ_R were determined from EMD simulations while the viscosity η was determined from NEMD simulations. The NEMD results reported here were obtained in the Newtonian regime, for a shear rate $\dot{\gamma} = 8.70 \times 10^{-4}$ ps^{-1}, which satisfies $\dot{\gamma} < \tau_R^{-1}$ for all n studied.

One set of EMD simulations was done at constant density for a series of chain lengths n. The density used was the bulk density for high molecular weight polyethylene, $\rho = 0.766$ g/cm^3 [9] and the simulations were carried out at ($T = 448$ K). Selected chain lengths at this state point were also studied with NEMD simulations. For small n, this state point corresponds to a high pressure state. In all of the constant density simulations (EMD and NEMD), interaction model A alone was employed. Another set of EMD simulations

were performed using the experimental densities at atmospheric pressure ($P \simeq 0.1$ MPa) for four chain lengths n. For each of these chain lengths, simulations were run using all three interaction models A, B, and C. These experimental density simulations were run at $T = 400$ K in order to remain far below the vapor-liquid critical temperature T_c for small n, which for example is 507 K for n-hexane and 617.5 K for n-decane [24]. Since we were interested in studying the effect of chain length on diffusion and viscosity, we chose temperatures which were higher than the melting temperature T_m for large n. For linear polyethylene, $T_m \simeq 400$ K. The lengths of the runs and the number of molecules used for each case are presented in Table III and Table IV.

To examine equilibrium structural statistics for $n > 66$, we used a continuum version of the RIS model for chains up to length $n = 2000$. There have been several studies [5,6,7,25,26] which have shown that by proper choice of the cutoff for the non-bonded interactions, the radius of gyration and end-to-end distance of an isolated chain compare very favorably with that of the melt. Here we followed the standard RIS model for polyethylene, which includes all bonded interactions and the 1-5 intramolecular Lennard-Jones potential (these are the "second-order interactions" of RIS theory and are known to be essential in order to reproduce the experimental characteristic ratio of the polyethylene chain). The main difference between the present model and the standard RIS model is that in the present implementation the molecule can explore the entire torsional potential surface, rather than being confined to a set of its minima. To allow comparison with the constant density EMD simulations, the simulations were done at $T = 448$ K. For short chains ($n \lesssim 100$), one can use Langevin dynamics simulations in which each isolated chain is coupled weakly to a heat bath. However for large n, the pivot algorithm [27] is considerably more efficient. Most of the results for the RIS simulation were obtained using the pivot algorithm, though for small n both methods gave comparable results as expected.

III. EQUILIBRIUM PROPERTIES

The structural properties for the molecules as expressed by the mean squared radius of gyration $\langle R_G^2 \rangle$, the two largest eigenvalues of the mass tensor l_I^2 and l_2^2, and the mean squared

end-to-end distance $\langle R^2 \rangle$ are collected in Tables III and IV for all the simulations. Results for $\langle R^2 \rangle / 6 \langle R_G^2 \rangle$ are shown in Fig. 2a for model A at $T = 448$ K. Data for both the EMD ($\rho = 0.766$ g/cm^3) and the RIS simulations are presented. Note that for small $n \lesssim 16$, this ratio increases with increasing n. For small n, the chains are relatively rigid. As such, the change in chain dimensions with increasing n is similar to what can be calculated for a linear string of uniform beads, where $\langle R^2 \rangle / 6 \langle R_G^2 \rangle$ goes from $\simeq 1$ for very small n to 2 for infinite n. Above $n \gtrsim 16$, flexibility of the chain becomes significant and $\langle R^2 \rangle / 6 \langle R_G^2 \rangle$ decreases with increasing n. A similar result was found by Baschnagel *et al.* [5] and Brown *et al.* [6]. The EMD results show that, for the values of n studied, the chains are clearly extended and non-Gaussian as $\langle R^2 \rangle > 6 \langle R_G^2 \rangle$. For this model and temperature, the crossover to Gaussian statistics occurs for n much greater than 100 in agreement with Baschnagel *et al.* [5], Brown *et al.* [6] and Paul *et al.* [7]. Figure 2a shows that the values of $\langle R^2 \rangle / 6 \langle R_G^2 \rangle$ predicted by RIS and EMD simulations agree within our statistical uncertainty. For the longest chain length studied, $n = 2000$, $\langle R^2 \rangle / 6 \langle R_G^2 \rangle$ is roughly 1% greater than the prediction for Gaussian chains for model A. A second order curve has been constructed on Fig. 2a representing the best fit of all the data for the RIS simulations and the data from the EMD simulations at $n = 66, 44, 36, 30, 24$, and 16. For model A, ($\langle R^2 \rangle / 6 \langle R_G^2 \rangle = 1 + 11.8/n - 93.4/n^2$). From this curve one can form an approximation of the chain length needed to reach Gaussian statistics within a given degree of error. For instance, the deviation from Gaussian statistics is less than 2% for chain lengths $n \gtrsim 600$ for model A. This is considerably larger than for a flexible chain consisting of beads connected with a spring [4] but with no torsional or bending forces, in which $\langle R^2 \rangle / 6 \langle R_G^2 \rangle = 1$ for $n \geq 10$.

From our previous studies for small n ($n \leq 24$), we expect that the actual crossover to Gaussian chain structural statistics will depend somewhat on the specific model, particularly through the parameters of the torsional potential. As discussed in Sec. II, the torsional potential for model A has a larger *gauche* bond energy than that used in models B and C (about 0.4 kcal/mol larger). This generally means that models B and C result in more thermodynamically flexible, and therefore more compact, molecules than model A. Data in

Table IV confirms these expectations; furthermore, the ranking of $\langle R^2 \rangle$ for the three models is constant with n: $\langle R^2 \rangle_A > \langle R^2 \rangle_C > \langle R^2 \rangle_B$. Comparing data for model A and model C, the influence of the *gauche* bond energy on $\langle R^2 \rangle$ is evident. This comparison is valid as models A and C represent the same implementation of the united atom model, only with different parameters. Furthermore, their largest difference in parameters, for this study of equilibrium properties, is found in their torsional potentials. Thus the effect on molecular size can be directly attributed to the difference in *gauche* bond energy. Comparing $\langle R^2 \rangle$ data for models B and C, we note that the difference in molecular size for the two models is larger than what one would expect due simply to the slight difference in the *gauche* bond energy. This is sensible since model B represents a fundamentally different parameterization of the united atom model than models A and C. This indicates that torsional potentials are not directly transferable between UA and AUA models. From observation of the data in Table IV, we anticipate that the crossover to Gaussian structural statistics with increasing n will occur first for model B, then for model C, and last for model A; Fig. 2b gives evidence of this. This figure is the same as Fig. 2a but with data from the EMD simulations using the three models at $T = 400$ K and experimental density at atmospheric pressure. While Fig. 2b shows only the beginning of the crossover, the ranking predicted is evident at this stage. The RIS simulations for the three models confirm the order of the crossover to Gaussian statistics.

Differences in the torsional potential also give rise to a difference in the expansion coefficient $k = d(\ln \langle R_G^2 \rangle)/dT$ between the models. In a previous publication [10], we found that for tetracosane around room temperature, $k = -1.1 \pm 0.2$ and $-0.6 \pm 0.3 \times 10^{-3}$ K^{-1} for model A and B, respectively. These results were for simulations run at the experimental density for $P = 0.1$ MPa for each temperature. This data was compared to the experimental value for bulk polyethylene $k = -1.07 \times 10^{-3}$ K^{-1} obtained from SANS measurements [28]. We can also consider previous data for $\langle R_G^2 \rangle$ of n-hexadecane [12] obtained at $T = 298, 323,$ and 373 K in conjunction with $\langle R_G^2 \rangle$ obtained at $T = 400$ K presented in this paper. From these, we can calculate $k = -0.8 \pm 0.2$ and $-0.6 \pm 0.1 \times 10^{-3}$ K^{-1} for n-hexadecane in model

A and B, respectively. These results are not presented to further evaluate the two models so much as to demonstrate that there is a very slow convergence of molecular sizes for models A and B with increasing temperature. In this respect, note that the average radius of gyration of n-hexadecane using model A at $T = 400$ K is still larger than the value for model B at 298 K [10]. While temperature can influence the position in n of the crossover to Gaussian statistics, these observations show that the model used has a much greater influence than temperature.

Boothroyd *et al.* [28] have reported on experimental data for the radius of gyration of a polyethylene chain in a melt. Specifically, they quote the radius of gyration for samples of molecular weight $M_W = 32000$ and 50000 in the temperature range of 380 K to 480 K. Dividing the experimental $\langle R_G^2 \rangle$ by M_W for $M_W = 32000$ and 50000 at 448 K, we obtain 0.23 and 0.19, respectively. In Fig. 3, $\langle R_G^2 \rangle / M_W$ is plotted versus $100/M_W^{1/2}$. Data obtained from both the EMD and RIS simulations at $T = 448$ K are shown for model A. In addition, a linear fit to all the RIS data and the EMD data for $30 \leq n \leq 66$ is also shown. Extrapolating this line to $M_W \to \infty$ gives a value of 0.28 for model A which is considerably larger than the experimental results for polyethylene. Similar fits to the RIS model using the parameters for models B and C give $\langle R_G^2 \rangle / M_W = 0.18$ and 0.24, respectively, in better agreement with experiment.

IV. DIFFUSION AND VISCOSITY RESULTS

Results for the self-diffusion constant D, the rotational diffusion time τ_R and the shear viscosity η are collected in Tables III and IV for all simulations performed. The self-diffusion constant is obtained from the slope of the mean-squared displacement of the molecular center of mass, averaged over all the molecules ($N_{\rm mol}$) in the system and all available initial times. In taking the average, the sum of the mean-squared displacements for the $N_{\rm mol}$ is divided by $N_{\rm mol} - 1$ to account for the fact that the center of mass of the system does not move. To calculate τ_R, we consider the first-order angular correlation of the longest principal axis of a molecule's ellipsoid of inertia [10]. At intermediate times, this correlation is well described by a simple exponential relaxation with a time constant τ_R as shown

in Fig. 4 for n-tetracosane and n-hexahexacontane. Equivalently, one can measure the autocorrelation function $\langle \mathbf{R}(t) \cdot \mathbf{R}(0) \rangle$ for the end-to-end distance [18] and fit this curve with the corresponding formula from the Rouse model [8] to obtain a measure of τ_R. Both of these correlations can be calculated from EMD. The viscosity was determined directly from NEMD simulations. From our previous study [12] comparing EMD and NEMD simulation methods for determining the viscosity of n-alkanes, the NEMD simulation technique requires about half the cpu time required by EMD methods for comparable accuracy. For further details see ref. [12].

The diffusion constants for the three models studied are compared to experimental data [29] for $T = 400$ K in Fig. 5. These simulations were run at the experimental densities listed in Table IV for $P = 0.1$ MPa. Note that for all of the simulation results as well as the experiments, the product Dn decreases with increasing n. This decrease is due to the fact that the density and therefore the monomeric friction coefficient ζ increases with increasing n, causing D at fixed T to decrease faster than predicted by the Rouse model. Assuming that the change in Dn is due to change in the monomeric friction coefficient a fit to the data gives $\zeta \sim n^{-0.8}$. One also sees from Fig. 5 and Table IV that model A overestimates D by approximately $15-50\%$, while models B and C fit the available experimental data quite well. Similar results for models A and B were found in our earlier studies [10,11,12] for n-decane, n-hexadecane, and n-tetracosane as well as for several branched alkanes. What is new in the current results is the agreement with experiment found for model C which is a symmetric united atom model. A symmetric united atom model is somewhat less computationally demanding to implement than an asymmetric united atom model. For identical length simulations we find that for 100 molecules of $n = 44$, the symmetric UA model requires approximately 10% less cpu time than the AUA model.

The three estimates of ζ are shown in Fig. 6 for constant density and $T = 448$ K. Note that ζ_D determined from the diffusion constant is only weakly dependent on n and even very small chain lengths give a reasonably good estimate of the friction coefficient of unentangled, Rouse-like chains. The change in ζ_D from $n = 10$ to 66 is only 10%. The significant change

in ζ with n at constant pressure as exhibited by the diffusion data discussed above all but disappears at constant density. This is in contrast with ζ_τ which depends much more strongly on n for small n; furthermore, $\zeta_\tau > \zeta_D$ [18]. The difference between $\zeta_\tau(R_G)$ and $\zeta_\tau(R)$ for small n is another representation of the deviation of equilibrium structural statistics from Rouse-like behavior. For $n \gtrsim 60$, all three methods of determining ζ agree within our statistical uncertainties as predicted by the Rouse model.

Another attribute of Fig. 6 warrants discussion. At small n, ζ_D decreases with increasing n and appears to reach a minimum around $n = 24$. This behavior is caused by an end effect: at small n, there is a large concentration of CH_3 united atoms whose Lennard-Jones ϵ parameter in model A is over twice that for CH_2 united atoms. An increase in ϵ is known to decrease diffusion [10] thereby effectively increasing ζ_D. To verify that this end effect caused the increase in ζ_D, the state points for $n = 6, 16$, and 24 were simulated but with the $\epsilon = 0.93$ kcal/mol for all the united atoms (i.e. the value for CH_2 in Model A). The mass of all united atom groups was that of CH_2 so the volumes were adjusted to achieve the stated density. The results for ζ_D are shown on Fig. 6 as filled symbols. The change in value at $n = 24$ is very small (4%) demonstrating that the end effect is nearly undetectable for large n as expected. The overall variation in ζ_D is now also smaller. From the three data points presented, it can be seen that the minimum in ζ_D with n still exists, however the minimum has shifted to $n = 16$, coincident with the position of the maximum in $\langle R_G^2 \rangle$ (Fig. 2a). This suggests that the origin of the minimum of ζ_d in Fig. 6 is related to the chain flexibility.

Finally, the three estimates for the viscosity are compared to our results from NEMD simulations in Fig. 7. As observed in our previous study [12], η_τ gives a very good estimate (within about 20%) for all n, while η_D is significantly smaller for small n. Since τ_R requires approximately ten times less cpu time to determine than η, we believe that at least for unentangled chains, τ_R is an efficient way to predict η without having to measure η directly. For $n \gtrsim 60$, all the estimates of η and the NEMD calculation agree within our statistical uncertainty.

V. CONCLUSIONS

The crossover to Rouse-like behavior for n-alkanes ($6 \leq n \leq 66$) as demonstrated by their self-diffusion constant D, viscosity η, and equilibrium structural statistics was studied numerically. For small n the chains were non-Gaussian and the mean squared end-to-end distance $\langle R^2 \rangle$ was greater than $6\langle R_G^2 \rangle$, where $\langle R_G^2 \rangle$ is the mean squared radius of gyration. As n increases, $\langle R^2 \rangle / \langle R_G^2 \rangle \to 6$ but only for n significantly larger than 200. At constant density, the Rouse model was used to extract the monomeric friction coefficient ζ and the viscosity η independently from the diffusion constant D and the longest relaxation time τ_R. ζ_D extracted from D was nearly independent of chain length while ζ_τ obtained from τ_R was much larger than ζ_D for small n. The viscosity measured in a non-equilibrium molecular dynamics simulation was closely approximated by the value of η determined from τ_R while the η inferred from D is smaller for small n. For $n \gtrsim 60$, the two estimates for both ζ and η agree as predicted from the Rouse model. Diffusion at normal pressure as calculated from three interaction models was studied for increasing n and the results were compared to experimental data. Very good agreement with experiment was found for two of the models while the third consistently overestimated D. For all models and experimental data, D was found to depend more strongly on n than predicted by Rouse theory.

REFERENCES

[1] P. E. Rouse, J. Chem. Phys. **21**, 1272 (1953).

[2] G. C. Berry and T. G. Fox, Adv. Polym. Sci. **5**, 261 (1968).

[3] J. D. Ferry, *Viscoelastic Properties of Polymers* (Wiley, New York, 1980).

[4] K. Kremer and G. S. Grest, J. Chem. Phys. **92**, 5057 (1990).

[5] J. Baschnagel, K. Qin, W. Paul, and K. Binder, Macromolecules **25**, 3117 (1992).

[6] D. Brown, J. H. R. Clarke, M. Okuda, and T. Yamazaki, J. Chem. Phys. **100**, 1684 (1994); J. Chem. Phys. **104**, 2078 (1996).

[7] W. Paul, G. D. Smith, and D. Y. Yoon, Macromolecules **00**, 00 (1998).

[8] M. Doi and S. F. Edwards, *The Theory of Polymer Dynamics* (Clarendon, Oxford, 1986).

[9] D. S. Pearson, G. ver Strate, E. von Meerwall, and F. C. Shilling, Macromolecules **20**, 1133 (1987).

[10] M. Mondello and G. S. Grest, J. Chem. Phys. **103**, 7156 (1995).

[11] M. Mondello, G. S. Grest, A. R. Garcia, and B. G. Silbernagel, J. Chem. Phys. **105**, 5208 (1996).

[12] M. Mondello and G. S. Grest, J. Chem. Phys. **106**, 9327 (1997).

[13] J. I. Siepmann, S. Karaboni, and B. Smit, Nature **365**, 330 (1993).

[14] B. Smit, S. Karaboni, and J. I. Siepmann, J. Chem. Phys. **102**, 2126 (1995).

[15] S. K. Nath, F. A. Escobedo, and J. J. de Pablo (to be published) recently showed that in the original calculations by Siepmann *el al.* [13,14] for the gas-liquid phase diagram, there was an error associated with the tail corrections for some of the thermodynamic properties computed. Nath *et al.* propose a slightly set of different parameters for the non-bonded Lennard-Jones interactions in model A to correct for this error. In this revised model, the

CH_3 united atoms for butane and longer n-alkanes are roughly 1% smaller than in model A and ϵ_{CH_3} and ϵ_{CH_2} are roughly 10% and 2% smaller than in model A, respectively. While these differences have an effect on the liquid-gas phase diagram for small n, they are not large enough to make a significant change in the self-diffusion constant and viscosity.

[16] P. Padilla and S. Toxvaerd, J. Chem. Phys. **94**, 5650 (1991).

[17] P. Padilla and S. Toxvaerd, J. Chem. Phys. **95**, 509 (1991).

[18] W. Paul, D. Y. Yoon, and G. D. Smith, J. Chem. Phys. **103**, 1702 (1995).

[19] In Ref. [18], the constrained bond length was 1.53 Å, $k_b = 120$ kcal/(mol rad^2), and $\theta_b = 110^o$. In addition, Paul, *et al* used a slightly different form of bending potential. The differences between these values and our implementation (see Table I) are minor.

[20] W. L. Jorgensen, J. D. Madura, and C. J. Swenson, J. Am. Chem. Soc. **106**, 6638 (1984).

[21] H. J. C. Berensen *et al.*, J. Chem. Phys. **81**, 3684 (1984).

[22] M. P. Allen and D. J. Tildesley, *Computer Simulation of Liquids* (Clarendon Press, Oxford, 1987).

[23] H. Andersen, J. Comput. Phys. **52**, 24 (1983).

[24] M. J. Anselme, M. Gude, and A. S. Teja, Fluid Phase Equilibria **57**, 317 (1990).

[25] R. G. Winkler, P. J. Ludovice, D. Y. Yoon, and H. Morawitz, J. Chem. Phys. **95**, 4709 (1991).

[26] A. Sariban, J. Brickmann, J. van Ruiten, and R. J. Meier, Macromolecules **25**, 5950 (1992).

[27] M. Lal, Molec. Phys. **17**, 57 (1969); B. MacDonald, N. Jan, D. L. Hunter, and M. O. Steinitz, J. Chem. Phys. **A18**, 2627 (1985); N. Madras and A. D. Sokal, J. Stat. Phys. **50**, 109 (1988).

[28] A. T. Boothroyd, A. R. Rennie, and C. B. Boothroyd, Europhys. Lett. **15**, 715 (1991).

[29] The experimental diffusion data for $n = 16$ and $n = 30$ are from T. Vardag, N. Kager, and H.-D. Lüdemann, Ber. Bunsenges. Phys. Chem. **95**, 859 (1991), for $n = 24$ from Mondello *et al.* [12] and for $n = 44$ from D. S. Pearson *et al.* [9]. All the data were obtained using PFG/NMR spectroscopy.

[30] J. H. Dymond, K. J. Young, and J. D. Isdale, J. Chem. Thermodynamics **11**, 887 (1979).

[31] J. H. Dymond, K. J. Young, and J. D. Isdale, Intl. J. of Thermophysics **1**, 345 (1980).

[32] API 42, *Properties of hydrocarbons of high molecular weight* (American Petroleum Institute, Research Project 42, Washington, DC, 1966).

[33] G. W. Nederbragt and J. W. M. Boelhouwer, Physica **13**, 305 (1947).

[34] A. K. Doolittle, J. of Chem. and Eng. Data **9**, 275 (1964).

FIG. 1. Comparison of torsional potential around $X - CH_2 - CH_2 - Y$ type bonds for models A, B, and C.

FIG. 2. Mean squared end-to-end distance $\langle R^2 \rangle$ divided by the radius of gyration $\langle R_G^2 \rangle$ versus n. For a Gaussian chain $\langle R^2 \rangle / 6 \langle R_G^2 \rangle = 1$. (a) $T = 448$ K and $\rho = 0.766$ g/cm^3. Data from model A for bulk and RIS simulations. (b) $T = 400$ K and experimental density at $P \simeq 0.1$ MPa. Data from models A, B, and C for bulk simulations.

FIG. 3. Radius of gyration $\langle R_G^2 \rangle$ divided by mass M versus $100/M^{1/2}$ for $T = 448$ K and $\rho = 0.766$ g/cm^3, model A bulk and RIS simulations for models A, B, and C.

FIG. 4. Time autocorrelation function of the orientation of the longest principal axis of inertia for n-tetracosane ($n = 24$) and n-hexahexacontane ($n = 66$) for $T = 448$ K. The solid line is for ($n = 24$) and the dashed is for ($n = 66$).

FIG. 5. Diffusion constant D from models A ($\Box$), B ($\triangle$), and C ($\circ$) for $T = 400$ K at the experimental densities listed in Table IV for $P = 0.1$ MPa. The experimental results ($\bullet$) are from ref. [29].

FIG. 6. Friction coefficients ζ versus n for $T = 448$ K. ζ_D ($\circ$) is extracted from the self-diffusion constant, eq. 6, while $\zeta_\tau(R)$ ($\Box$) and $\zeta_\tau(R_G)$ ($\triangle$) are determined from the longest relaxation time τ_R, eq. 7. The filled symbol ($\bullet$) is ζ_D obtained from simulations for chains consisting entirely of CH_2 united atoms.

FIG. 7. Viscosity η_τ ($\circ$) determined from the longest relaxation time τ_R, eq. 5, and $\eta_D(R)$ ($\Box$) and $\eta_D(R_G)$ ($\triangle$) determined from the self-diffusion constant D, eq. 8, versus n for $T = 448$ K. Also shown for four values of n is the viscosity η ($\bullet$) measured in our non-equilibrium molecular dynamics simulations.

TABLE I. Intramolecular interaction parameters.

	Model A (UA[a])	Model B (AUA[b])	Model C (UA[c])	Units
bond length	1.54	1.54	1.54	$\AA$
k_b (bending)	124.18	124.28	124.18	kcal/(mol rad^2)
θ_b	114.0^o	114.6^o	114.0^o	
a_0 (torsion)	2.007	2.062	1.736	kcal/mol
a_1	4.012	4.821	4.500	
a_2	0.271	0.162	0.764	
a_3	-6.290	-6.218	-7.000	
a_4		-0.324		
a_5		-0.502		

[a]Intramolecular parameters for n-alkanes from Ref. [13,14]. Torsional potentials are taken from Ref. [20].

[b]Intramolecular parameters from Ref. [16]; torsional potential (d) was used.

[c]The torsional potential is the "modified" one from Ref. [18]. The bending term used here is slightly different from the one used by Paul *et al*; see [19].

TABLE II. Lennard-Jones potential parameters.

Model	Group	σ ($\AA$)	ϵ (kcal/mol)	d ($\AA$)
A (UA[a])	CH_3	3.930	0.227	
	CH_2	3.930	0.093	
B (AUA[b])	CH_3	3.527	0.238	0.275
	CH_2	3.527	0.159	0.370
C (UA[c])	CH_3	4.010	0.227	
	CH_2	4.010	0.093	

[a]From Ref. [13,14].

[b]From Ref. [16].

[c]The value used in Ref. [18] for ϵ_{CH_3} was 0.226 kcal/mol and the σ for both CH_3 and CH_2 united atoms was 4.009$\AA$.

TABLE III. Summary of the constant density ($\rho = 0.766$ g/cm^3) simulation results for model A at $T = 448$ K. Results for the mean squared radius of gyration $\langle R_G^2 \rangle$ and the end-to-end distance $\langle R^2 \rangle$ are expressed in $\mathring{A}^2$. The eigenvalues of the mass tensor (l_I^2) satisfy the equality $\langle R_G^2 \rangle = l_1^2 + l_2^2 + l_3^2$, with $l_1^2 > l_2^2 > l_3^2$. Results for the self-diffusion and rotational relaxation time τ_R are from equilibrium molecular dynamics simulations, while the results for the viscosity η are from non-equilibrium molecular dynamics simulations. The total length of the run and the number of molecules used are also shown. Uncertainties in the last reported digit(s) are given in parenthesis.

	n	N	t (ns)	$\langle R_G^2 \rangle$	$l_1^2/\langle R_G^2 \rangle$	$l_2^2/\langle R_G^2 \rangle$	$\langle R^2 \rangle$	D (10^{-6}cm^2/sec)	τ_R (ps)
EMD	6	64	1.0	4.39(1)	0.897(1)	0.082(1)	31.9(1)	25.8(7)	11
	10	64	1.5	10.7(1)	0.900(1)	0.082(1)	87.5(2)	22.7(7)	33
	16	64	1.5	23.5(1)	0.876(1)	0.105(1)	194(1)	15.5(7)	86
	24	100	1.0	44.1(2)	0.847(2)	0.130(2)	353(3)	11.2(5)	176
	30	100	1.5	61.8(4)	0.833(3)	0.140(2)	484(6)	8.56(31)	260
	36	100	2.0	79.8(7)	0.821(3)	0.148(3)	605(10)	6.40(34)	360
	44	100	2.0	104(1)	0.804(4)	0.159(3)	758(16)	5.27(30)	513
	66	100	14.0	178(1)	0.785(2)	0.170(2)	1240(17)	3.12(8)	1140

	n	N	t (ns)	η (cP)
NEMD	16	100	18.5	0.967(70)
	30	64	18.0	1.56(6)
	44	100	13.5	2.30(5)
	66	100	10.1	3.22(5)

TABLE IV. Summary of the simulations at the experimental density for $P \simeq 0.1$ MPa and $T = 400$ K. For each chain length, data is presented from simulations employing models A, B, and C. Densities ρ are quoted in gm/cm^3. The results for the mean squared radius of gyration $\langle R_G^2 \rangle$ and the end-to-end distance $\langle R^2 \rangle$ are expressed in $\mathring{A}^2$. The eigenvalues of the mass tensor (l_I^2) satisfy the equality $\langle R_G^2 \rangle = l_1^2 + l_2^2 + l_3^2$, with $l_1^2 > l_2^2 > l_3^2$. The total length of the run and the number of molecules used are also shown. Uncertainties in the last reported digit(s) are given in parenthesis.

Substance	Model	N	t (ns)	$\langle R_G^2 \rangle$	$l_1^2/\langle R_G^2 \rangle$	$l_2^2/\langle R_G^2 \rangle$	$\langle R^2 \rangle$	D	D_{exp}
n-C_{16}	A	64	2.0	24.1(1)	0.881(1)	0.102(1)	201(1)	23.2(1.3)	20(1)
$\rho = 0.6999$[a]	B	64	2.0	21.8(1)	0.858(1)	0.119(1)	173(1)	18.1(9)	
	C	64	2.0	23.3(1)	0.876(1)	0.105(1)	192(1)	18.5(1.0)	
n-C_{24}	A	100	1.0	45.3(3)	0.852(3)		367(5)	12.9(9)	8.23(82)
$\rho = 0.7260$[b]	B	100	1.0	40.1(4)	0.833(4)		309(6)	8.90(62)	
	C	100	2.0	43.3(2)	0.845(2)	0.131(2)	344(3)	9.11(28)	
n-C_{30}	A	64	4.0	64.0(4)	0.838(2)	0.137(2)	507(5)	8.62(47)	5.2(3)
$\rho = 0.7421$[c]	B	64	4.0	55.3(4)	0.820(3)	0.148(2)	415(5)	5.30(30)	
	C	64	4.0	61.0(4)	0.833(3)	0.140(2)	477(6)	6.03(34)	
n-C_{44}	A	100	4.0	111(1)	0.815(3)	0.152(3)	833(15)	4.52(21)	2.4(2)
$\rho = 0.7570$[d]	B	100	4.0	92.3(1.2)	0.794(4)	0.165(3)	654(15)	2.49(12)	
	C	100	4.0	104(1)	0.807(4)	0.157(3)	765(16)	3.17(17)	

[a]Experimental densities at ten temperatures were obtained from Ref. [30,31,32] and used to create a linear extrapolation to $T = 400$ K.

[b]From Ref. [33].

[c]Obtained by a linear interpolation between experimental densities from Ref. [34].

[d]Calculated based on information from Ref. [18]. While no experimental reference is given in Ref. [18], a comparison of the value used was made to the value obtained by a linear interpolation between data from Ref. [32]. The two values differed by $< 1\%$.

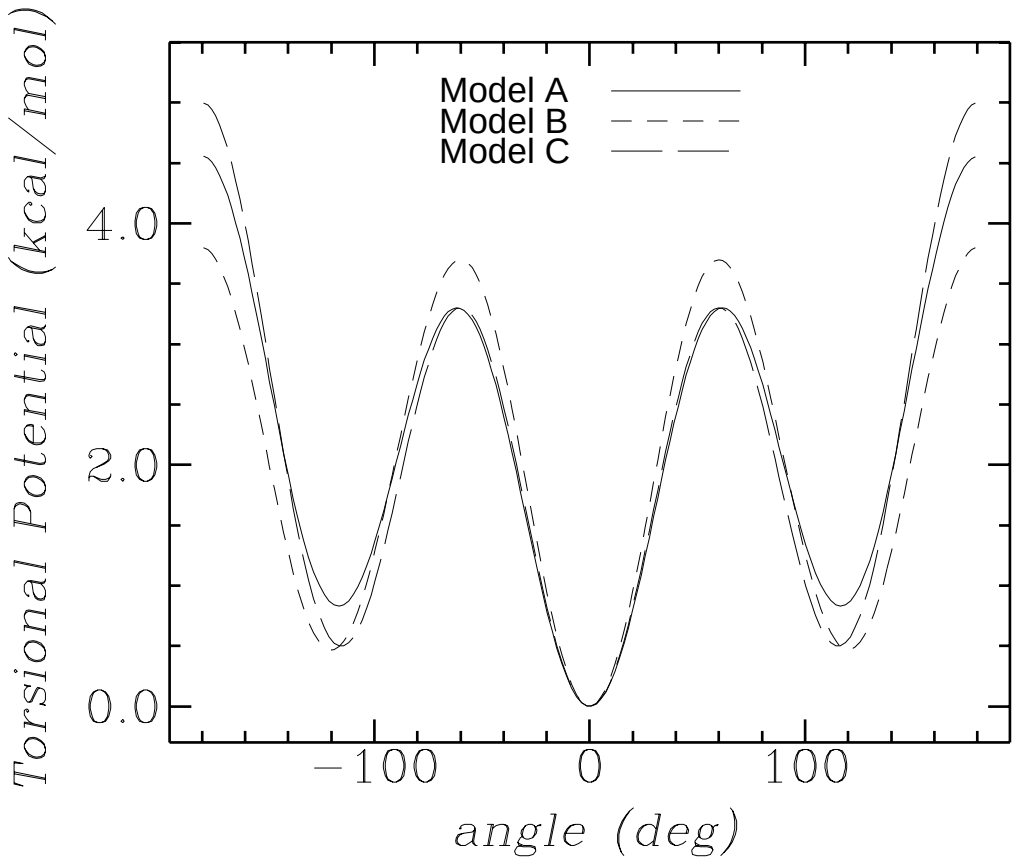
Model A
Model B
Model C
Torsional Potential (kcal/mol)
4.0
2.0
0.0
−100
0
100
angle (deg)

Figure 1

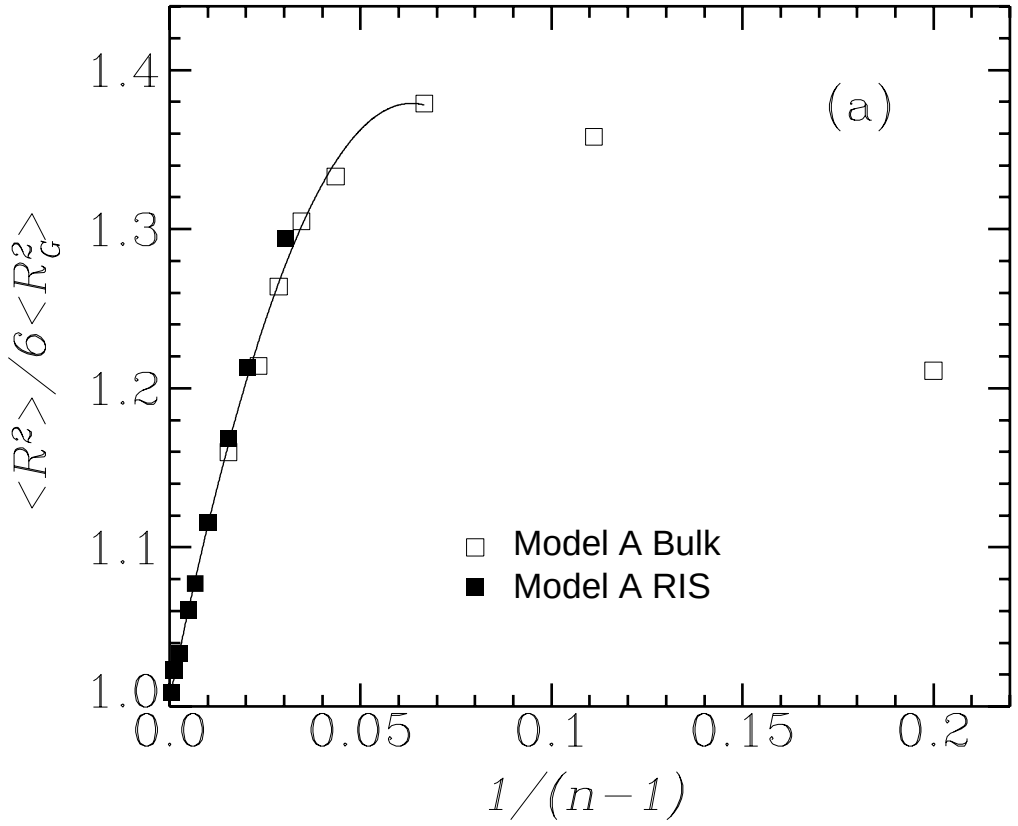
(a)
Model A Bulk
Model A RIS
$<R^2>/6<R_G^2>$
$1/(n-1)$
1.0
1.1
1.2
1.3
1.4
0.0
0.05
0.1
0.15
0.2

Figure 2(a)

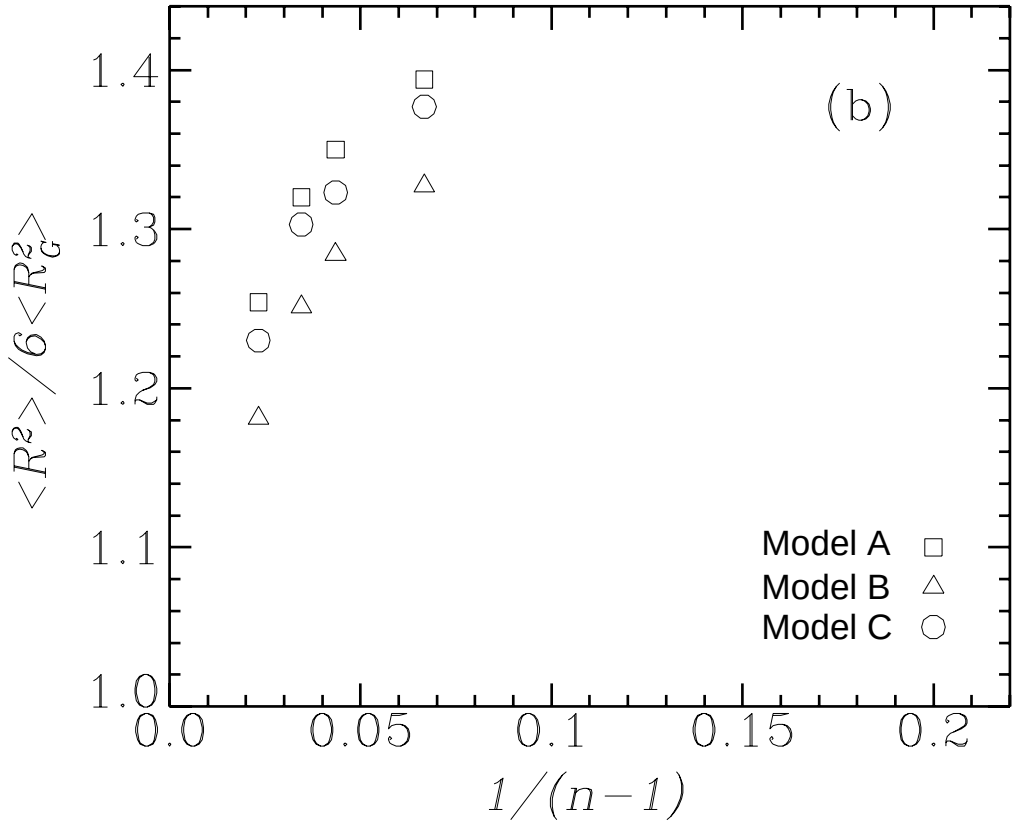
(b)
Model A
Model B
Model C
$<R^2>/6<R_G^2>$
$1/(n-1)$
1.0
1.1
1.2
1.3
1.4
0.0
0.05
0.1
0.15
0.2

Figure 2(b)

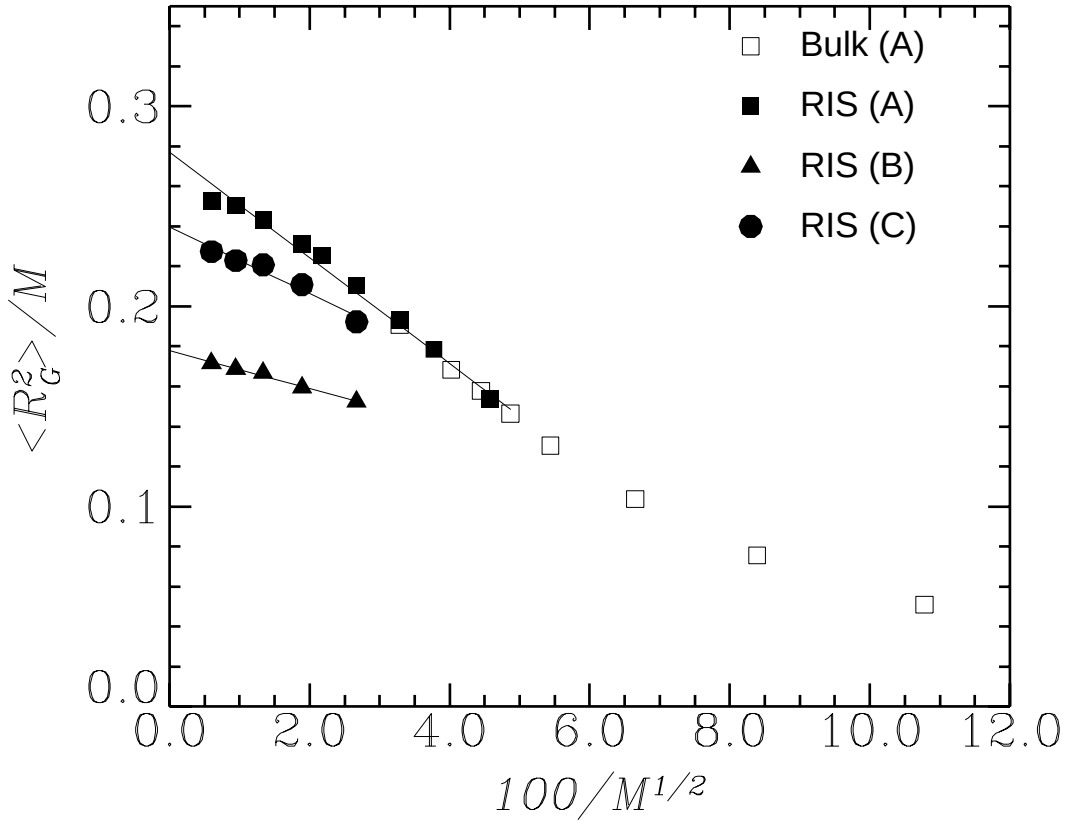
Bulk (A)
RIS (A)
RIS (B)
RIS (C)
0.3
0.2
0.1
0.0
0.0
2.0
4.0
6.0
8.0
10.0
12.0
$<R_G^2>/M$
$100/M^{1/2}$

Figure 3

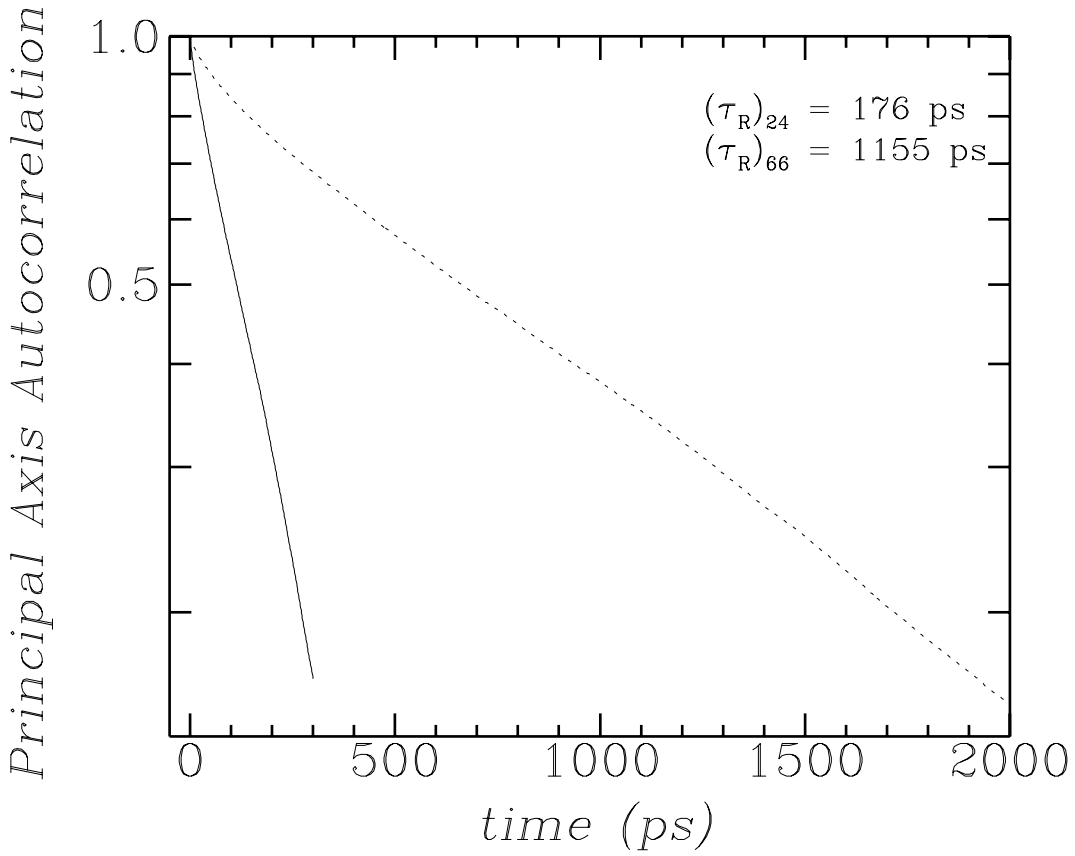
Principal Axis Autocorrelation
1.0
0.5
0
500
1000
1500
2000
time (ps)
$(\tau_R)_{24}$ = 176 ps
$(\tau_R)_{66}$ = 1155 ps

Figure 4

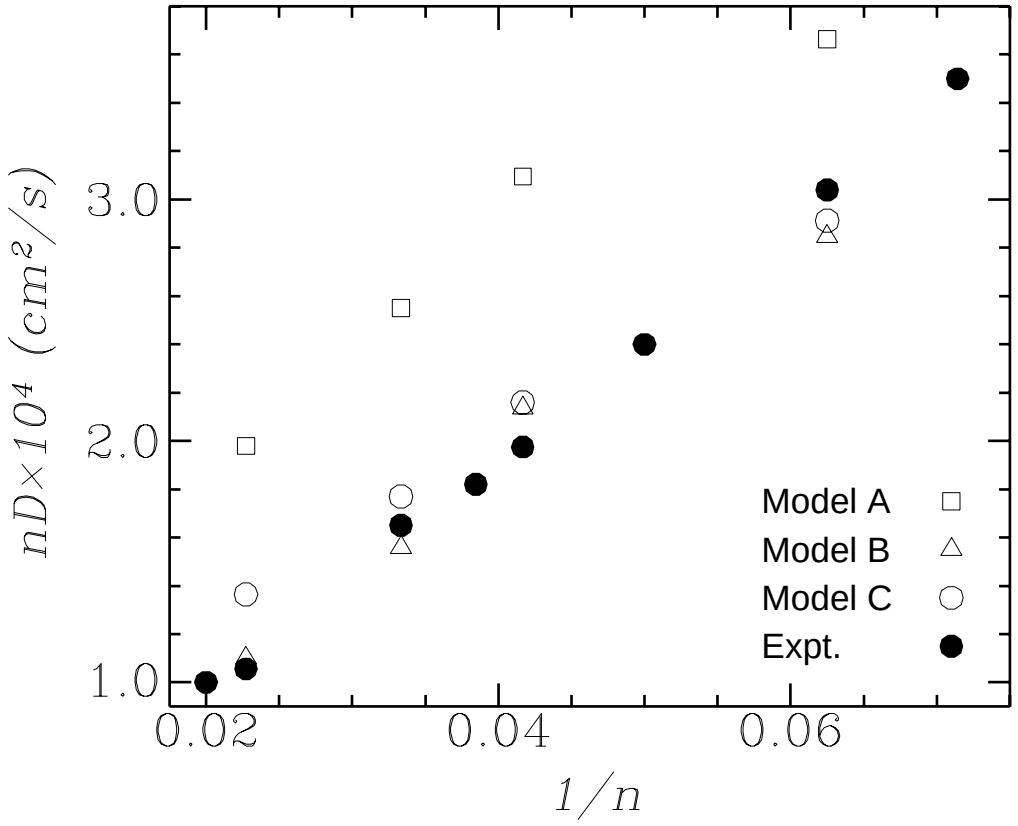

Figure 5

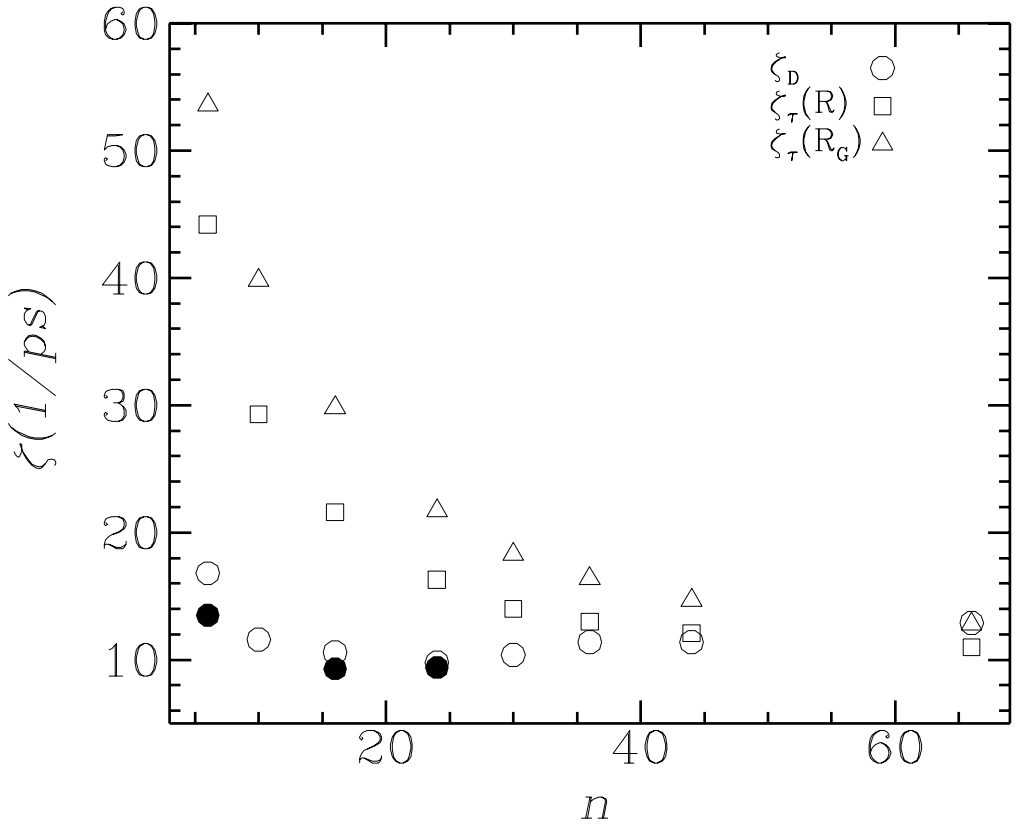

Figure 6

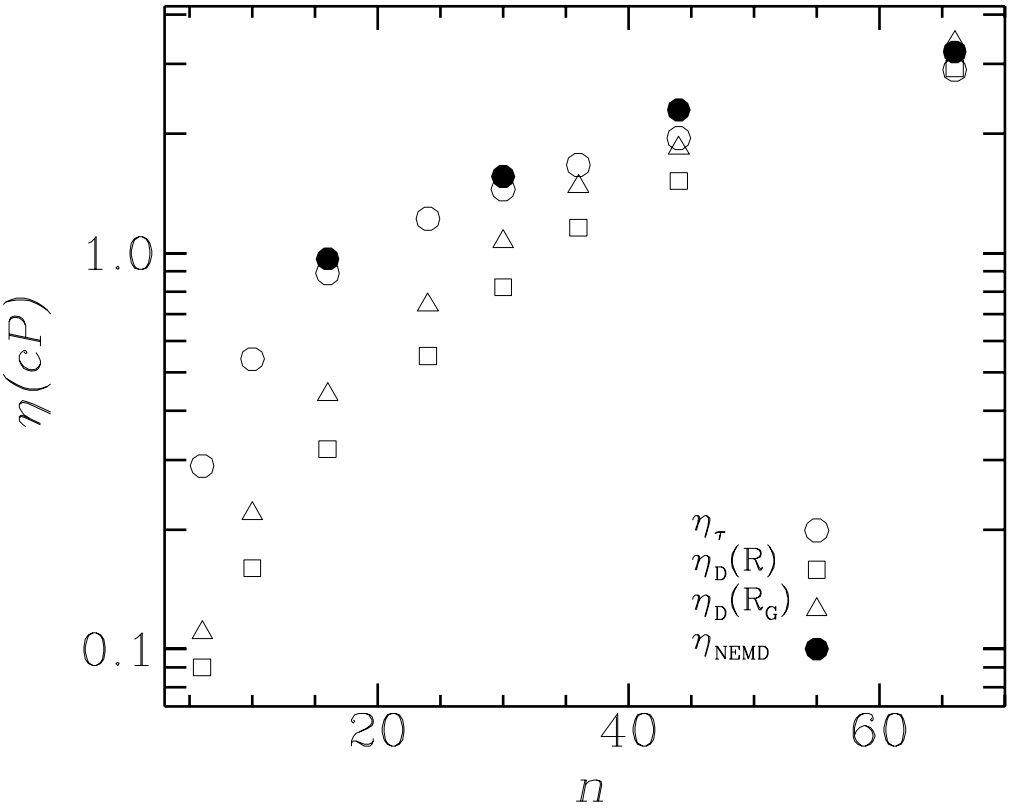

Figure 7